INTERNATIONAL JOURNAL FOR NUMERICAL METHODS IN ENGINEERING
Int. J. Numer. Meth. Engng 2009; **80**:403–424
Published online 8 June 2009 in Wiley InterScience (www.interscience.wiley.com). DOI: 10.1002/nme.2641

Mixed piezoelectric plate elements with direct evaluation of transverse electric displacement

E. Carrera[‡] and P. Nali[*,†]

Aerospace Department, Politecnico di Torino, Corso Duca degli Abruzzi, 24, 10129 Torino, Italy

SUMMARY

A mixed variational statement for the analysis of layered structures under the effect of mechanical and electrical fields is proposed in this paper to develop finite plate elements that permit the direct evaluation of transverse electrical displacement D_z. The original Reissner mixed variational theorem, RMVT, has been modified to account for 'only' interlaminar continuous D_z. Continuity of mechanical variables, such as transverse shear and normal stress components, has been discarded to provide a simple 'electrical' modified RMVT, here called RMVT-D_z. Finite element implementations are made via the Carrera unified formulation. The advantages of the proposed approach have been demonstrated through numerical comparisons with classical formulations based on the principle of virtual displacements as well as with available 3D solutions. Copyright © 2009 John Wiley & Sons, Ltd.

Received 24 September 2008; Revised 30 January 2009; Accepted 6 April 2009

KEY WORDS: finite elements; multilayered plates; multifield problems; refined models; smart structures

1. INTRODUCTION

Smart systems can be considered as the candidates for next generation structures in aerospace vehicles as well as for some advanced products in the automotive and ship industries. Piezoelectric materials are extensively used in this framework. These materials are characterized by the so-called 'direct' and 'inverse effect': an applied electrical potential induces mechanical stresses and vice-versa. Such an electro-mechanical coupling permits one to build closed-loop control systems in which piezo materials play the role of both actuators and sensors. An intelligent structure can therefore be built in which, for instance, deformations or vibrations are reduced by appropriate control laws.

[*]Correspondence to: P. Nali, Aerospace Department, Politecnico di Torino, Corso Duca degli Abruzzi, 24, 10129 Torino, Italy.
[†]E-mail: pietro.nali@polito.it
[‡]Professor.

Contract/grant sponsor: European Space Agency, ESTEC; contract/grant number: 21082/06/NL/PA

An appropriate use of piezoelectric materials, however, requires an accurate description of the electrical and mechanical fields in the constitutive layers. The present paper focuses on the computational, finite element (FE), electro-mechanical two-dimensional modeling of smart structures embedding piezo layers.

Piezoelectric plates appear as multilayered structures. Very often, piezoelectric layers are embedded in laminated structures made of anisotropic composite materials. The importance of appropriate modeling of piezoelectric plates is clearly displayed by the large number of papers that have been published over the last two decades.

Among the available review papers, those by Saravanos and Heyliger [1], and Wang and Yan [2] are herein mentioned. A short review of some of the latest contributions to the FE analysis of piezoelectric plates follows. A FE that includes an FSDT description of displacements and a layer-wise (LW) form of the electric potential was developed by Sheik *et al.* [3]. The numerical, membrane and bending behavior of FEs that are based on FSDTs were analyzed by Auricchio *et al.* [4] in the framework of a suitable variational formulation. The third-order theory of HOT type was applied by Thornburg and Chattopadhyay [5] to derive FEs that take into consideration the electro-mechanical coupling. Similar elements have more recently been considered by Shu [6]. The extension of the third-order zig-zag Ambartsumian multilayered theory to finite analysis of electro-mechanical problems has been proposed by Oh and Cho [7]. An extension to piezoelectricity of numerically efficient plate/shell elements based on the mixed interpolation of tensorial components formulation has recently been provided by Kögl and Bucalem [8, 9].

Although traditional LW theories, based on the principle of virtual displacements (PVD) are able to accurately predict mechanical displacements, electric potential, in-plane stress and in-plane electric displacements; they are unable to guarantee the continuity of transverse stresses or of the transverse electric displacement at the interface between two adjacent layers (the continuity of transverse stresses should be enforced for equilibrium reasons). The continuity conditions for secondary variables, such as transverse stresses and transverse electric displacement, are known in the literature as C_z^0 requirements [10]. These requirements can be satisfied by employing the mixed approach. In particular, displacement components, electric potential, transverse stresses and transverse electric displacement can be independently considered and used as degrees of freedom, using the Reissner mixed variational theorem (RMVT) [11, 12]. In this way, the continuity of transverse stresses and of the transverse electric displacement is always guaranteed and, consequently, the C_z^0 requirements are automatically fulfilled. During the last decade, the first author and his co-workers have contributed extensively to the application of RMVT to multilayered structures and they have introduced a LW FE formulation for composite plates that fulfill the continuity of transverse stresses between layers [13]. Closed-form solution analysis as well as FE applications [14] have shown that RMVT can be considered as a very suitable tool to provide a quasi-3D description of stress and strain fields in anisotropic-laminated structures. The formulation employed in these latter works, named Carrera unified formulation (CUF), permits one to formulate both equivalent single layer (ESL) and LW models in terms of a few 'Fundamental Nuclei' whose form does not depend on either the order of the through-the-thickness expansion that has been used for the various variables or on the number of nodes of the element. Many works have been devoted to the extension of the CUF. Among others, Carrera [15] extends PVD and RMVT variational statements to piezo-laminated plates. The modeling of piezo-laminated plates using LW mixed FEs was then proposed in [16]. Subsequently, an extension of the RMVT to piezoelectric laminates with analytical results was published in [17]. Mixed FEs for static and dynamics analysis of piezoelectric plates have been provided in [18], where only transverse stresses were modeled by RMVT.

DOI: 10.1002/nme

The related variational statement has been named P-RMVT, where 'P' stands for 'Partial'. In this case, the transverse electric displacement D_z was calculated by post-processing. More accurate results for the evaluation of the D_z have recently been provided in [19], where the transverse stresses, together with the D_z, have been modeled by RMVT. The employed variational statement has been called F-RMVT, where the 'F' stands for 'Full'.

Among the various variables, the evaluation of the transverse electric displacement is of particular interest. The D_z is, in fact, closely related to the electrical charge Q

$$Q = \int_{\Omega} D_z \, \mathrm{d}\Omega \tag{1}$$

where Ω is the plate surface. The charge consists of a fundamental input/output in a closed-loop control of a smart structure. Faster and accurate evaluation of Q is a key point in the development of an efficient and reliable closed-loop control algorithm. However, D_z, in classical applications is only given '*a posteriori*' via post-processing of the primary variables (the displacements and the electrical potential). An extended RMVT application, with D_z assumed as primary variable, has been employed in this paper, which has been called RMVT-D_z. The relevant difference between RMVT-D_z and the above-mentioned F-RMVT is that the first does not imply the modeling of transverse stresses, while both variational statements require the modeling of the transverse electric displacement. As a consequence, RMVT-D_z leads to a lower computational effort than F-RMVT and it assures, at the same time, accurate results for the transverse electric displacement. An almost complete overview of the possible subcases of RMVT was given in [20]. The RMVT-D_z in the latter work was mentioned as a possible extension of RMVT to piezoelectric structures. However, constitutive equations and FE matrices consistent with RMVT-D_z were not given in [20]. The present work derives the constitutive equations for RMVT-D_z and develops applications for plate elements in the framework of the CUF. The RMVT-D_z fundamental nucleus (explicitly given in the Appendix) contains information to build the corresponding stiffness matrix and in this paper is presented and numerically assessed.

2. CONSIDERED VARIATIONAL STATEMENTS

2.1. The PVD for the electro-mechanical case

The PVD statement for the pure mechanical case study is commonly written as follows:

$$\int_V (\delta \boldsymbol{\varepsilon}_G^{\mathrm{T}} \boldsymbol{\sigma}_H) \, \mathrm{d}V = \delta L_e \tag{2}$$

where superscript 'T' indicates the array transposition, δ is the variational symbol and bold letters denote arrays. The subscripts 'G' and 'H' indicate variables obtained by geometrical relations and by constitutive/Hooke's relations, respectively. σ, ε and L_e indicate stresses, strains and the external work in the same sequence.

In the case of applied electro-mechanical loading on a surface Ω, employing Einstein's summation convention over repeated indices, the virtual variation of the external work can be expressed as

$$\delta L_e = \int_{\Omega} (\bar{t}_i \, \delta u_i - \bar{Q} \, \delta \phi) \, \mathrm{d}\Omega \tag{3}$$

DOI: 10.1002/nme

where $\bar{t}_i$ is the mechanical loading in ith direction (pressure), u_i is the displacement component in ith direction, $\bar{Q}$ is the charge density on the plate surface and ϕ is the electric potential.

Stresses and strains are conveniently split between in-plane and out-of-plane (normal or transverse) components [20]

$$\int_V (\delta\boldsymbol{\varepsilon}_{pG}^{\mathrm{T}}\ \boldsymbol{\sigma}_{pH} + \delta\boldsymbol{\varepsilon}_{nG}^{\mathrm{T}}\,\boldsymbol{\sigma}_{nH})\,\mathrm{d}V = \delta L_e \tag{4}$$

with

$$\boldsymbol{\varepsilon}_p^{\mathrm{T}} = \{\varepsilon_{xx}\ \ \varepsilon_{yy}\ \ \varepsilon_{xy}\},\quad \boldsymbol{\sigma}_p^{\mathrm{T}} = \{\sigma_{xx}\ \ \sigma_{yy}\ \ \sigma_{xy}\},\quad \boldsymbol{\varepsilon}_n^{\mathrm{T}} = \{\varepsilon_{zz}\ \ \varepsilon_{xz}\ \ \varepsilon_{yz}\},\quad \boldsymbol{\sigma}_n^{\mathrm{T}} = \{\sigma_{zz}\ \ \sigma_{xz}\ \ \sigma_{yz}\}$$

Cartesian x, y, z reference system is considered and notation already used in previous work [19] is referred to: subscript 'p' denotes in-plane unknowns and subscript 'n' denotes out-of-plane unknowns; subscript 'z' indicates through-the-thickness z-direction, while subscripts 'x' and 'y' are for the two in-plane directions.

If electrical contributions are included, the PVD in Equation (4) becomes

$$\int_V (\delta\boldsymbol{\varepsilon}_{pG}^{\mathrm{T}}\,\boldsymbol{\sigma}_{pH} + \delta\boldsymbol{\varepsilon}_{nG}^{\mathrm{T}}\,\boldsymbol{\sigma}_{nH}\delta - \delta\mathbf{E}_{pG}^{\mathrm{T}}\,\mathbf{D}_{pH} - \delta E_{nG}\,D_{nH})\,\mathrm{d}V = \delta L_e \tag{5}$$

with

$$\mathbf{E}_p^{\mathrm{T}} = \{E_x\ \ E_y\},\quad \mathbf{D}_p^{\mathrm{T}} = \{D_x\ \ D_y\},\quad E_n = \{E_z\},\quad D_n = \{D_z\}$$

where D and E indicate the transverse electric displacement and the electric field, respectively.

The condensed vectorial notation already discussed in [20] is employed in the present work. The two multifield variables are introduced as

$$\mathscr{S}^{\mathrm{T}} = \{\sigma_{xx}\ \ \sigma_{yy}\ \ \sigma_{xy}\ \ -D_x\ \ -D_y\ \ \sigma_{zz}\ \ \sigma_{xz}\ \ \sigma_{yz}\ \ -D_z\} \tag{6}$$

$$\mathscr{E}^{\mathrm{T}} = \{\varepsilon_{xx}\ \ \varepsilon_{yy}\ \ \varepsilon_{xy}\ \ E_x\ \ E_y\ \ \varepsilon_{zz}\ \ \varepsilon_{xz}\ \ \varepsilon_{yz}\ \ E_z\} \tag{7}$$

where $\mathscr{S}$ is the vector of extensive variables and $\mathscr{E}$ is the vector of intensive ones. D_z and D_n are the same quantities expressed in different notations.

It is possible to rewrite Equation (5) in the form as simple as Equation (2) for multifield problems:

$$\int_V (\delta\mathscr{E}_G^{\mathrm{T}}\,\mathscr{S}_H)\,\mathrm{d}V = \delta L_e \tag{8}$$

2.2. *The RMVT-D_z*

The advantage of using RMVT lies in the possibility of assuming two independent set of variables: a set of primary unknowns and a set of extensive variables, which are modeled in the thickness plate z-direction. This leads to the '*a priori*' and complete fulfillment of the interlaminar continuity for the modeled extensive variables, with consequent satisfaction of the C_z^0 requirements in [13]. As stated in the introduction, the RMVT has been commonly employed to obtain accurate results for transverse stresses in pure mechanical problems [11]. In piezoelectric applications, RMVT has been recently extended to model the transverse electric displacement other than normal stresses [18].

DOI: 10.1002/nme

This work represents the first application of the RMVT with only the electric displacement D_z modeled in the thickness plate z-direction. The convenience of that is explained in the introduction.

The RMVT statement with '*a priori*' modeling of the transverse electric displacement D_z (or D_n) is here called RMVT-D_z and it appears in the literature in the following form [20]:

$$\int_V (\delta\boldsymbol{\varepsilon}_{pG}^{\mathrm{T}}\,\boldsymbol{\sigma}_{pH} + \delta\boldsymbol{\varepsilon}_{nG}^{\mathrm{T}}\,\boldsymbol{\sigma}_{nH} - \delta\mathbf{E}_{pG}^{\mathrm{T}}\,\mathbf{D}_{pH} - \delta E_{nG}\,D_n - \delta D_n(E_{nG} - E_{nH}))\,\mathrm{d}V = \delta L_e \tag{9}$$

By referring to the condensed notation and considering that subscript 'a' indicates 'not modeled quantities', whereas subscripts 'b' are related to 'modeled quantities', the following vectors can be introduced:

$\mathscr{S}_{aH} = \{\sigma_{xx}\ \sigma_{yy}\ \sigma_{xy}\ -D_x\ -D_y\ \sigma_{zz}\ \sigma_{xz}\ \sigma_{yz}\}_H$ is the vector of not-modeled extensive variables, which are calculated by constitutive relations;

$\mathscr{S}_b = \{-D_z\}$ is the vector of modeled extensive variables;

$\mathscr{E}_{aG} = \{\varepsilon_{xx}\ \varepsilon_{yy}\ \varepsilon_{xy}\ E_1\ E_2\ \varepsilon_{zz}\ \varepsilon_{xz}\ \varepsilon_{yz}\}_G$ is the vector of intensive variables associated with $\mathscr{S}_a$ and calculated by geometrical relations;

$\mathscr{E}_{bG} = \{E_z\}_G$ is the vector of intensive variables associated with $\mathscr{S}_b$ and calculated by geometrical relations;

$\mathscr{E}_{bH} = \{E_z\}_H$ is the vector of intensive variables associated with $\mathscr{S}_b$ and calculated by constitutive relations.

In so doing, the RMVT statement with '*a priori*' modeling of the transverse electric displacement D_z takes the following form:

$$\int_V (\delta\mathscr{E}_{aG}^{\mathrm{T}}\,\mathscr{S}_{aH} + \delta\mathscr{E}_{bG}^{\mathrm{T}}\,\mathscr{S}_b^k + \delta\mathscr{S}_b^{\mathrm{T}}(\mathscr{E}_{bG} - \mathscr{E}_{bH}))\,\mathrm{d}V = \delta L_e \tag{10}$$

In the next section, the constitutive relations are obtained for the RMVT-D_z variational statement, both in traditional notation, in accordance with Equation (9), and in the condensed notation, in accordance with Equation (10).

3. CONSTITUTIVE RELATIONS

Physical constitutive equation, which is suitable for PVD applications, for the electro-mechanical case reduces to

$$\begin{aligned} \sigma_{ij} &= C_{ijlm}\varepsilon_{lm} - e_{ijl}E_l \\ D_l &= e_{lij}\varepsilon_{ij} + \varepsilon_{lm}E_m \end{aligned} \tag{11}$$

where standard tensor notation is used and Einstein's summation convention is implied over repeated indices and with C_{ijlm} is the elastic coefficients—Hooke's law; e_{lij} the piezoelectric coefficients; ε_{ij} the permittivity coefficients. Note that $2\varepsilon_{ij}$ components in tensorial notation correspond to ε_{ij} components in vectorial notation, when $i \neq j$.

Passing from indices to vectors in split form (in-plane and out-of-plane components), constitutive variables become: $\boldsymbol{\sigma}_p$, $\boldsymbol{\sigma}_n$, $\boldsymbol{\varepsilon}_p$, $\boldsymbol{\varepsilon}_n$, $\mathbf{E}_p$, E_n, $\mathbf{D}_p$, D_n, where E_n and D_n are scalars.

DOI: 10.1002/nme

Equation (11) can be rewritten as in [19]

$$\begin{aligned}
\boldsymbol{\sigma}_p &= \mathbf{C}_{pp}\boldsymbol{\varepsilon}_p + \mathbf{C}_{pn}\boldsymbol{\varepsilon}_n - \mathbf{e}_{pp}^{\mathrm{T}}\mathbf{E}_p - \mathbf{e}_{np}^{\mathrm{T}}E_n \\
\boldsymbol{\sigma}_n &= \mathbf{C}_{pn}^{\mathrm{T}}\boldsymbol{\varepsilon}_p + \mathbf{C}_{nn}\boldsymbol{\varepsilon}_n - \mathbf{e}_{pn}^{\mathrm{T}}\mathbf{E}_p - \mathbf{e}_{nn}^{\mathrm{T}}E_n \\
\mathbf{D}_p &= \mathbf{e}_{pp}\boldsymbol{\varepsilon}_p + \mathbf{e}_{pn}\boldsymbol{\varepsilon}_n + \varepsilon_{pp}\mathbf{E}_p + \varepsilon_{pn}E_n \\
D_n &= \mathbf{e}_{np}\boldsymbol{\varepsilon}_p + \mathbf{e}_{nn}\boldsymbol{\varepsilon}_n + \varepsilon_{pn}^{\mathrm{T}}\mathbf{E}_p + \varepsilon_{nn}E_n
\end{aligned} \tag{12}$$

where matrices $\mathbf{C}_{pp}$, $\mathbf{C}_{pn}$, $\mathbf{C}_{nn}$, $\mathbf{e}_{pp}$, $\mathbf{e}_{pn}$, $\mathbf{e}_{nn}$, ε_{pp}, ε_{pn} and ε_{nn} contain the constitutive coefficients in Equation (11), which are already rotated to the physical reference system and are partitioned so that the in-plane quantities are split from the out-of-plane ones (see [17, 21] for the explicit form).

Variationally consistent constitutive relations must be derived according to Equation (9). To do that, the system in Equation (12) is rearranged. First, the normal component of an electric field is obtained

$$E_n = \varepsilon_{nn}^{-1}(D_n - \mathbf{e}_{np}\boldsymbol{\varepsilon}_p - \mathbf{e}_{nn}\boldsymbol{\varepsilon}_n - \varepsilon_{pn}^{\mathrm{T}}\mathbf{E}_p) \tag{13}$$

that is:

$$E_n = -\varepsilon_{nn}^{-1}\mathbf{e}_{np}\boldsymbol{\varepsilon}_p - \varepsilon_{nn}^{-1}\mathbf{e}_{nn}\boldsymbol{\varepsilon}_n - \varepsilon_{nn}^{-1}\varepsilon_{pn}^{\mathrm{T}}\mathbf{E}_p + \varepsilon_{nn}^{-1}D_n \tag{14}$$

Substituting Equation (14) into (12) and keeping Equation (14) as the last equation, RMVT-D_z constitutive relations are obtained:

$$\begin{aligned}
\boldsymbol{\sigma}_p &= (\mathbf{C}_{pp} + \mathbf{e}_{np}^{\mathrm{T}}\varepsilon_{nn}^{-1}\mathbf{e}_{np})\boldsymbol{\varepsilon}_p + (\mathbf{C}_{pn} + \mathbf{e}_{np}^{\mathrm{T}}\varepsilon_{nn}^{-1}\mathbf{e}_{nn})\boldsymbol{\varepsilon}_n + (-\mathbf{e}_{pp}^{\mathrm{T}} + \mathbf{e}_{np}^{\mathrm{T}}\varepsilon_{nn}^{-1}\varepsilon_{pn}^{\mathrm{T}})\mathbf{E}_p + (-\mathbf{e}_{np}^{\mathrm{T}}\varepsilon_{nn}^{-1})D_n \\
\boldsymbol{\sigma}_n &= (\mathbf{C}_{pn}^{\mathrm{T}} + \mathbf{e}_{nn}^{\mathrm{T}}\varepsilon_{nn}^{-1}\mathbf{e}_{np})\boldsymbol{\varepsilon}_p + (\mathbf{C}_{nn} + \mathbf{e}_{nn}^{\mathrm{T}}\varepsilon_{nn}^{-1}\mathbf{e}_{nn})\boldsymbol{\varepsilon}_n + (-\mathbf{e}_{pn}^{\mathrm{T}} + \mathbf{e}_{nn}^{\mathrm{T}}\varepsilon_{nn}^{-1}\varepsilon_{pn}^{\mathrm{T}})\mathbf{E}_p + (-\mathbf{e}_{nn}^{\mathrm{T}}\varepsilon_{nn}^{-1})D_n \\
\mathbf{D}_p &= (\mathbf{e}_{pp} - \varepsilon_{pn}\varepsilon_{nn}^{-1}\mathbf{e}_{np})\boldsymbol{\varepsilon}_p + (\mathbf{e}_{pn} - \varepsilon_{pn}\varepsilon_{nn}^{-1}\mathbf{e}_{nn})\boldsymbol{\varepsilon}_n + (\varepsilon_{pp} - \varepsilon_{pn}\varepsilon_{nn}^{-1}\varepsilon_{pn}^{\mathrm{T}})\mathbf{E}_p + (\varepsilon_{pn}\varepsilon_{nn}^{-1})D_n \\
E_n &= -\varepsilon_{nn}^{-1}\mathbf{e}_{np}\boldsymbol{\varepsilon}_p - \varepsilon_{nn}^{-1}\mathbf{e}_{nn}\boldsymbol{\varepsilon}_n - \varepsilon_{nn}^{-1}\varepsilon_{pn}^{\mathrm{T}}\mathbf{E}_p + \varepsilon_{nn}^{-1}D_n
\end{aligned} \tag{15}$$

A more compact expression of Equation (15) can be obtained by substituting matrices' products with a new set of constitutive coefficients, denoted by the 'hat'.

$$\begin{aligned}
\boldsymbol{\sigma}_p &= \widehat{\mathbf{C}}_{pp}\boldsymbol{\varepsilon}_p + \widehat{\mathbf{C}}_{pn}\boldsymbol{\varepsilon}_n + \widehat{\mathbf{e}}_{pp}^{\mathrm{T}}\mathbf{E}_p + \widehat{\mathbf{e}}_{np}^{\mathrm{T}}D_n \\
\boldsymbol{\sigma}_n &= \widehat{\mathbf{C}}_{pn}^{\mathrm{T}}\boldsymbol{\varepsilon}_p + \widehat{\mathbf{C}}_{nn}\boldsymbol{\varepsilon}_n + \widehat{\mathbf{e}}_{pn}^{\mathrm{T}}\mathbf{E}_p + \widehat{\mathbf{e}}_{nn}^{\mathrm{T}}D_n \\
\mathbf{D}_p &= \widehat{\mathbf{e}}_{pp}\boldsymbol{\varepsilon}_p + \widehat{\mathbf{e}}_{pn}\boldsymbol{\varepsilon}_n + \widehat{\varepsilon}_{pp}\mathbf{E}_p + \widehat{\varepsilon}_{pn}D_n \\
E_n &= \widehat{\mathbf{e}}_{np}\boldsymbol{\varepsilon}_p + \widehat{\mathbf{e}}_{nn}\boldsymbol{\varepsilon}_n + \widehat{\varepsilon}_{pn}^{\mathrm{T}}\mathbf{E}_p + \widehat{\varepsilon}_{nn}D_n
\end{aligned} \tag{16}$$

Constitutive relations in Equation (16) are suitable for the application of the RMVT variational statement in the form of Equation (9).

If the variational statement of Equation (10) is addressed, constitutive relations are obtained as follows, according to the condensed notation.

For the sake of clarity, it is convenient to specify that primary unknown variables are collected in the vector as

$$\mathbf{V}^{kT} = \{u_x^k \;\; u_y^k \;\; u_z^k \;\; \phi^k \;\; D_z^k\}$$

where the superscript k states for the kth layer.

DOI: 10.1002/nme

It is useful to rewrite vectors introduced in Section 2.2:

$$\mathscr{E}_a^{kT} = \{\varepsilon_{xx}^k \;\; \varepsilon_{yy}^k \;\; \varepsilon_{xy}^k \;\; E_x^k \;\; E_y^k \;\; \varepsilon_{zz}^k \;\; \varepsilon_{xz}^k \;\; \varepsilon_{yz}^k\}, \quad \mathscr{E}_b^{kT} = \{E_z^k\}$$

$$\mathscr{S}_a^{kT} = \{\sigma_{xx}^k \;\; \sigma_{yy}^k \;\; \sigma_{xy}^k \;\; -D_x^k \;\; -D_y^k \;\; \sigma_{zz}^k \;\; \sigma_{xz}^k \;\; \sigma_{yz}^k\}, \quad \mathscr{S}_b^{kT} = \{-D_z^k\}$$

The following geometrical relations can be written as:

$$\mathscr{E}_{aG}^k = \mathbf{D}_a \mathbf{V}^k \tag{17}$$

$$\mathscr{E}_{bG}^k = \mathbf{D}_b \mathbf{V}^k \tag{18}$$

$$\mathscr{S}_{bG}^k = \mathbf{D}_{b'} \mathbf{V}^k \tag{19}$$

In explicit form:

$$\mathbf{D}_a = \begin{pmatrix} \partial_x & 0 & 0 & 0 & 0 \\ 0 & \partial_y & 0 & 0 & 0 \\ \partial_y & \partial_x & 0 & 0 & 0 \\ 0 & 0 & 0 & -\partial_x & 0 \\ 0 & 0 & 0 & -\partial_y & 0 \\ 0 & 0 & \partial_z & 0 & 0 \\ \partial_z & 0 & \partial_x & 0 & 0 \\ 0 & \partial_z & \partial_y & 0 & 0 \end{pmatrix}, \quad \mathbf{D}_b = (0 \;\; 0 \;\; 0 \;\; -\partial_z \;\; 0), \quad \mathbf{D}_{b'} = (0 \;\; 0 \;\; 0 \;\; 0 \;\; -1)$$

Referring to the condensed notation and specifying which quantities are obtained by Hooke's law or by geometrical relations, Equation (16) becomes:

$$\tilde{\mathscr{S}}_H^k = \tilde{\mathbf{H}}^k \tilde{\mathscr{E}}_G^k \tag{20}$$

$\tilde{\mathscr{S}}_H^k$ is composed by the vector of not-modeled extensive variables $\mathscr{S}_{aH}^k$ and the vector of intensive variables $\mathscr{E}_{bH}$ (which is associated with $\mathscr{S}_b^k$); $\tilde{\mathscr{E}}_G^k$ is composed by the vector of intensive variables $\mathscr{E}_{aG}^k$ (which is associated with $\mathscr{S}_a^k$) and the vector of modeled extensive variables $\mathscr{S}_b^k$, which can be thought as a geometrical vector by Equation (19):

$$\tilde{\mathscr{S}}_H^{kT} = \{\mathscr{S}_{aH}^{kT} \;\; \mathscr{E}_{bH}^{kT}\}, \quad \tilde{\mathscr{E}}_G^{kT} = \{\mathscr{E}_{aG}^{kT} \;\; \mathscr{S}_{bG}^{kT}\}$$

The physical constitutive matrix $\mathbf{H}^k$ can be partitioned by dividing cells related to modeled and not-modeled quantities

$$\mathbf{H}^k = \begin{Bmatrix} \mathbf{H}_{aa}^k & \mathbf{H}_{ab}^k \\ \mathbf{H}_{ba}^k & \mathbf{H}_{bb}^k \end{Bmatrix} \tag{21}$$

where $\mathbf{H}_{ab}^k = \mathbf{H}_{ba}^{kT}$.

DOI: 10.1002/nme

In explicit form:

$$\mathbf{H}^k_{aa}=\begin{pmatrix} C^k_{11} & C^k_{12} & C^k_{16} & 0 & 0 & C^k_{13} & 0 & 0 \\ C^k_{12} & C^k_{22} & C^k_{26} & 0 & 0 & C^k_{23} & 0 & 0 \\ C^k_{16} & C^k_{26} & C^k_{66} & 0 & 0 & C^k_{36} & 0 & 0 \\ 0 & 0 & 0 & -\varepsilon^k_{11} & -\varepsilon^k_{12} & 0 & 0 & 0 \\ 0 & 0 & 0 & -\varepsilon^k_{12} & -\varepsilon^k_{22} & 0 & 0 & 0 \\ C^k_{13} & C^k_{23} & C^k_{36} & 0 & 0 & C^k_{33} & 0 & 0 \\ 0 & 0 & 0 & 0 & 0 & 0 & C^k_{55} & C^k_{45} \\ 0 & 0 & 0 & 0 & 0 & 0 & C^k_{45} & C^k_{44} \end{pmatrix}, \quad \mathbf{H}^k_{ab}=\begin{pmatrix} -e^k_{31} \\ -e^k_{32} \\ -e^k_{36} \\ 0 \\ 0 \\ -e^k_{33} \\ 0 \\ 0 \end{pmatrix}$$

$$\mathbf{H}^k_{ba}=(-e^k_{31}\ -e^k_{32}\ -e^k_{36}\ 0\ 0\ -e^k_{33}\ 0\ 0), \quad \mathbf{H}^k_{bb}=(-\varepsilon^k_{33})$$

Physical constitutive relations can be arranged according to the above partitioning:

$$\mathcal{S}^k_{aH}=\mathbf{H}^k_{aa}\mathcal{E}^k_{aG}+\mathbf{H}^k_{ab}\mathcal{E}^k_{bG}, \quad \mathcal{S}^k_{bH}=\mathbf{H}^k_{ba}\mathcal{E}^k_{aG}+\mathbf{H}^k_{bb}\mathcal{E}^k_{bG} \tag{22}$$

From Equations (22) one has

$$\mathcal{S}^k_{aH}=\widetilde{\mathbf{H}}^k_{aa}\mathcal{E}^k_{aG}+\widetilde{\mathbf{H}}^k_{ab}\mathcal{S}^k_{bG}, \quad \mathcal{E}^k_{bH}=\widetilde{\mathbf{H}}^k_{ba}\mathcal{E}^k_{aG}+\widetilde{\mathbf{H}}^k_{bb}\mathcal{S}^k_{bG} \tag{23}$$

with:

$$\widetilde{\mathbf{H}}^k_{aa}=\mathbf{H}^k_{aa}-\mathbf{H}^k_{ab}(\mathbf{H}^k_{bb})^{-1}\mathbf{H}^k_{ba}, \quad \widetilde{\mathbf{H}}^k_{ab}=\mathbf{H}^k_{ab}(\mathbf{H}^k_{bb})^{-1}, \quad \widetilde{\mathbf{H}}^k_{ba}=-(\mathbf{H}^k_{bb})^{-1}\mathbf{H}^k_{ba}, \quad \widetilde{\mathbf{H}}^k_{bb}=(\mathbf{H}^k_{bb})^{-1}$$

The matrix $\widetilde{\mathbf{H}}^k$ of Equation (20) is:

$$\widetilde{\mathbf{H}}^k=\begin{Bmatrix} \widetilde{\mathbf{H}}^k_{aa} & \widetilde{\mathbf{H}}^k_{ab} \\ \widetilde{\mathbf{H}}^k_{ba} & \widetilde{\mathbf{H}}^k_{bb} \end{Bmatrix} \tag{24}$$

It is to be noticed that matrix $\widetilde{\mathbf{H}}^k$ represents the constitutive relations suitable for the RMVT-D_z in the form of Equation (10) and it contains the same information of the system in Equation (16). See the Appendix 7 for the explicit form of $\widetilde{\mathbf{H}}^k$.

The advantage of using the condensed notation is that the above shown procedure to calculate constitutive relations is applicable also when different/more extensive variables are modeled through the thickness plate z-direction and then it represents a general and an automatic way to calculate the constitutive coefficients for many different cases of variational statements, as explained in [20].

4. THROUGH-THE-THICKNESS ASSUMPTIONS OF PRIMARY VARIABLES VIA CUF

In the framework of the CUF [22], the primary unknowns are assumed by using a generalized expansion:

$$\mathbf{V}^k(x,y,z)=F_\tau(z)\,\mathbf{V}^k_\tau(x,y), \quad \tau=0,1,\ldots,N \tag{25}$$

DOI: 10.1002/nme

The repeated indexes are summed over their ranges. The polynomials $F_\tau(z)$ constitute a set of independent functions. Such a base is arbitrarily chosen: power of z, Lagrange polynomials or a combination of Legendre polynomials can be considered. N denotes the order of the introduced expansion. In case of RMVT-D_z application, variables concerning displacements, electrical potential and transverse electric displacement are included in vector $\mathbf{V}^k$.

It is understood that, by the arbitrary choice of the thickness expansion, the same computational code can address not just one FE, but a complete family of them with different descriptions for primary unknowns along the thickness of the structure. In so doing, the CUF reduces a three-dimensional problem to a two-dimensional problem. Meanwhile, the order of the expansion along the thickness of the plate is taken as a free parameter of the FE and, in the developed code, it can be changed ranging from 1 up to 4.

By appropriately choosing the thickness functions, both an ESL and an LW description along the thickness of the plate is admissible. In an ESL model, a global assumption for the unknowns is considered along the thickness of the plate (i.e. a Taylor expansion) while, in an LW model, the expansion is made for each layer separately and then interlaminar continuity conditions are enforced by the assembly procedure. The latter leads generally to more accurate results, but the number of the nodal degrees of freedom increases with the number of the layers coming out to a greater computational cost.

In the implemented code, for an LW theory the thickness functions are defined by

$$F_t = \frac{P_0 + P_1}{2}, \quad F_b = \frac{P_0 - P_1}{2}, \quad F_r = P_r - P_{r-2}, \ \ r = 2, \ldots, N \tag{26}$$

where $P_i = P_i(\zeta_k)$ is the *Legendre* polynomial of the ith order defined in the domain $-1 \leqslant \zeta_k \leqslant 1$. The chosen thickness functions have the interesting properties:

$$\zeta_k = \begin{cases} 1 : F_t = 1, & F_b = 0, \quad F_r = 0 \\ -1 : F_t = 0, & F_b = 1, \quad F_r = 0 \end{cases} \tag{27}$$

Using these definitions, the generalized assumptions for the primary unknowns of the kth layer in Equation (25) can be stated as:

$$\mathbf{V}^k(x, y, z) = F_b(z)\mathbf{V}_b^k(x, y) + F_r(z)\mathbf{V}_r^k(x, y) + F_t(z)\mathbf{V}_t^k(x, y) = F_\tau \mathbf{V}_\tau^k$$
$$\text{with } r = 2, \ldots, N \tag{28}$$

The variables $\mathbf{V}_b$ and $\mathbf{V}_t$ are the actual primary unknowns at the bottom and the top surfaces of the layer and the inter-laminar continuity can be easily imposed:

$$\mathbf{V}_t^k = \mathbf{V}_b^{(k+1)} \quad \text{with } k = 1, \ldots, N_l - 1 \tag{29}$$

Acronyms are used for the implemented plate elements. These are denoted by LM1, LM2, LM3, LM4 in which: L states that an LW description is employed and M indicates that a mixed approach based on RMVT is used; 1–4 denotes the order of the expansion introduced for the field variables in each layer (from first to fourth order). When acronyms EM1, EM2, EM3, EM4 are used, an ESL description is employed. LD1, LD2, LD3, LD4 and ED1, ED2, ED3, ED4 are the corresponding acronyms when the classical approach based on PVD is used (letter D).

DOI: 10.1002/nme

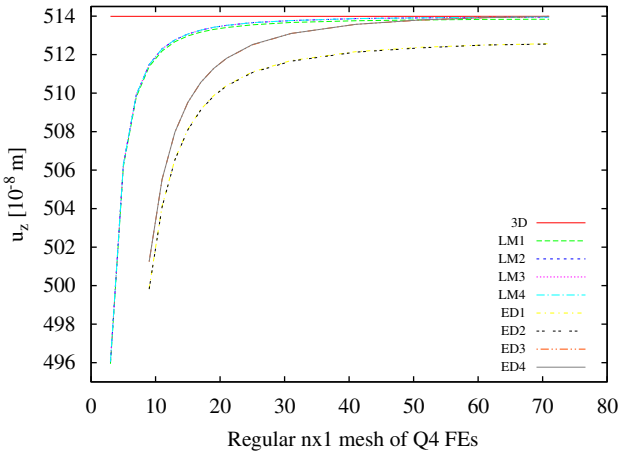

Figure 1. Midplane transverse displacement at the center of the plate: convergence study.

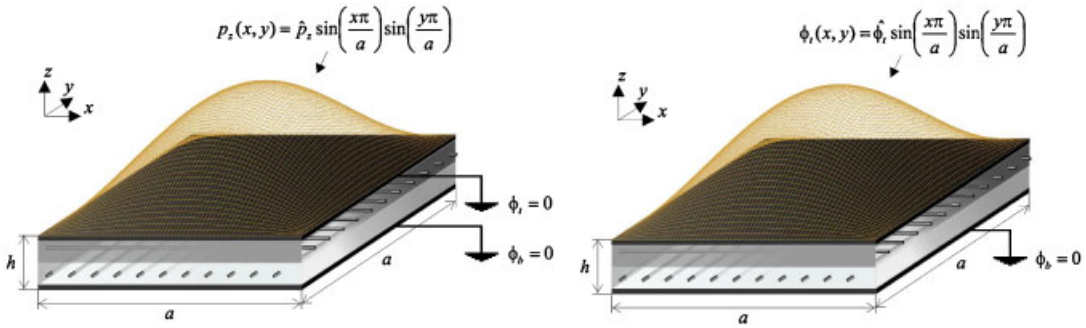

Figure 2. On the left the plate in sensor configuration (applied pressure); on the right the plate in actuator configuration (applied potential).

5. 'FUNDAMENTAL NUCLEI' AND FE MATRICES

This section is devoted to the RMVT-D_z variational statement, while the application of the corresponding PVD can be found in [20].

5.1. *FE discretization*

In the case of FEM implementation, unknowns can be expressed in terms of their nodal values, via the shape functions N_i

$$\mathbf{V}_\tau^k(x,y) = N_i(x,y)\mathbf{R}_{\tau i}^k, \quad i = 1,2,\ldots,N_n \tag{30}$$

while for the virtual variations

$$\delta\mathbf{V}_s^k(x,y) = N_j(x,y)\delta\mathbf{R}_{sj}^k, \quad j = 1,2,\ldots,N_n \tag{31}$$

DOI: 10.1002/nme

Table I. PVD and RMVT-D_z results: comparison between LD2 and LM2 FEM solutions with the 3D-exact solution, sensor case.

	$u_2 \times 10^{12}$	$u_2 \times 10^{12}$	$u_2 \times 10^{12}$	$\phi \times 10^{1}$	$\phi \times 10^{1}$	$\phi \times 10^{1}$
Height	3D [24]	PVD	RMVT-D_z	3D [24]	PVD	RMVT-D_z
1.000	−47.549	−45.593	−45.594	0.0000	0.0000	0.0000
0.975	−41.425	−39.527	−39.528	0.0189	0.0181	0.0181
0.950	−35.424	−33.567	−33.569	0.0358	0.0336	0.0336
0.925	−29.531	−27.715	−27.772	0.0488	0.0464	0.0464
0.900	−23.732	−21.969	−21.970	0.0598	0.0567	0.0567
0.800	−10.480	−10.058	−10.577	0.0589	0.0560	0.0559
0.700	0.1413	−0.0836	−0.0836	0.0589	0.0560	0.0559
0.600	9.8917	9.5104	9.5108	0.0596	0.0567	0.0567
0.500	20.392	18.205	18.206	0.0611	0.0583	0.0583
0.400	24.768	22.149	22.150	0.0634	0.0606	0.0605
0.300	29.110	26.700	26.703	0.0665	0.0637	0.0637
0.200	33.819	31.860	31.863	0.0706	0.0677	0.0677
0.100	39.309	37.628	37.632	0.0756	0.0726	0.0726
0.075	44.492	42.930	42.934	0.0602	0.0581	0.0581
0.050	49.772	48.341	48.346	0.0425	0.0411	0.0411
0.025	55.163	53.863	53.867	0.0224	0.0218	0.0218
0.000	60.678	59.494	59.499	0.0000	0.0000	0.0000

Displacements are in (m); electric potential is in (V). $u_2 = u_2(a/2, 0)$; $\phi = \phi(a/2, b/2)$.

where N_n denotes the number of nodes concerning the considered FE and $\mathbf{R}^k_{\tau i}$ is the vector containing nodal values of unknowns:

$$\mathbf{R}^{kT}_{\tau i} = \{R^k_{u_1 \tau i} \quad R^k_{u_2 \tau i} \quad R^k_{u_3 \tau i} \quad R^k_{\phi \tau i} \quad R^k_{D_3 \tau i}\} \tag{32}$$

The final expression of the unknowns is:

$$\mathbf{V}^k(x, y, z) = F_\tau N_i \mathbf{R}^k_{\tau i} \tag{33}$$

5.2. *Derivation of fundamental nuclei and FE matrices*

Upon substitution of Equations (17), (18), (19), (23) and (31), the variational statement in Equation (10) leads to a set of equilibrium equations which can be formally put in the following compact form:

$$\delta \mathbf{R}^k_{sj} : \mathbf{K}^{k\tau sij} \mathbf{R}^k_{\tau i} = \mathbf{P}^k_{sj} \tag{34}$$

where $\mathbf{P}^k$ is the vector of nodal loads and the related boundary conditions are $\overline{\mathbf{R}}^k$.

The number of obtained equations coincides with the number of introduced variables: τ and s vary from 0 to N, i and j vary from 1 to N_n and k ranges from 1 to N_l.

Matrix $\mathbf{K}^{k\tau sij}$ is the fundamental nucleus. In this case, it is a 5×5 array and, more in general, it provides the information to build the stiffness matrix (see the Appendix 7 for the explicit form of $\mathbf{K}^{k\tau sij}$).

Whatever is the considered variational statement, starting from the fundamental nucleus, for a given discretization, the stiffness matrix $\mathbf{K}$ can be calculated by numerical integration and the

DOI: 10.1002/nme

Table II. PVD and RMVT-D_z results: comparison between LD2 and LM2 FEM solutions with the 3D-exact solution, sensor case.

	$\sigma_{33}\times10^1$	$\sigma_{33}\times10^1$	$\sigma_{33}\times10^1$	σ_{22}	σ_{22}	σ_{22}	σ_{12}	σ_{12}	σ_{12}
Height	3D [24]	PVD	RMVT-D_z	3D [24]	PVD	RMVT-D_z	3D [24]	PVD	RMVT-D_z
1.000	10.000	9.6313	9.6381	6.5643	6.2392	6.2387	−2.4766	−2.3547	−2.3546
0.975	9.9657	9.4336	9.4354	5.8201	5.5033	5.5030	−2.1824	−2.0680	−2.0679
0.950	9.8682	9.3631	9.3598	5.0855	4.7857	4.7856	−1.8942	−1.7866	−1.7864
0.925	9.7154	9.4197	9.4112	4.3595	4.0865	4.0866	−1.6114	−1.5103	−1.5102
0.900	9.5151	9.6034	9.5898	3.6408	3.4057	3.4059	−1.3332	−1.2393	−1.2392
0.900	9.5151	10.163	10.163	2.8855	3.8364	3.8362	−0.2463	−0.2290	−0.2290
0.800	8.5199	8.7018	8.7018	1.4499	2.0094	2.0093	−0.1534	−0.1475	−0.1474
0.700	7.3747	7.4395	7.4395	0.2879	0.3332	0.3332	−0.0817	−0.0776	−0.0775
0.600	6.1686	6.3764	6.3764	−0.7817	−1.1923	−1.1922	−0.0212	−0.0193	−0.0193
0.500	4.9831	5.5124	5.5124	−1.9266	−2.5670	−2.5669	0.0369	0.0274	0.0274
0.500	4.9831	4.9178	4.9179	0.0991	0.0527	0.0527	0.0369	0.0274	0.0274
0.400	3.8045	3.9244	3.9244	−0.0149	−0.0683	−0.0683	0.0965	0.0771	0.0771
0.300	2.6137	2.8259	2.8259	−0.1280	−0.2049	−0.2049	0.1529	0.1335	0.1335
0.200	1.4821	1.6223	1.6223	−0.2426	−0.3571	−0.3570	0.2139	0.1966	0.1966
0.100	0.4868	0.3136	0.3136	−0.3616	−0.5248	−0.5247	0.2882	0.2663	0.2663
0.100	0.4868	0.8251	0.8365	−4.2348	−3.9325	−3.9325	1.5603	1.4415	1.4413
0.075	0.2845	0.9872	0.9436	−4.8806	−4.5636	−4.5634	1.8105	1.6933	1.6931
0.050	0.1312	1.0311	1.0339	−5.5337	−5.2123	−5.2119	2.0651	1.9499	1.9498
0.025	0.0340	0.9568	0.9553	−6.1951	−5.8785	5.8780	2.3246	2.2115	2.2113
0.000	0.0000	0.7641	0.7583	−6.8658	−6.5623	−6.5617	2.5899	2.4779	2.4777

Stresses are in (Pa). $\sigma_{33}=\sigma_{33}(a/2,b/2)$; $\sigma_{11}=\sigma_{11}(a/2,b/2)$; $\sigma_{12}=\sigma_{12}(0,0)$.

assembly procedure. **K** is the representative of the Gibbs-free energy contribution and it should be emphasized that, regardless of its name, the stiffness matrix contains information pertaining to all the considered fields and not just to the mechanical field. If a static analysis is required, the system to solve is the following:

$$\mathbf{KR}=\mathbf{P} \tag{35}$$

where **P** is the vector of nodal loads and **R** is the vector of nodal unknowns.

6. NUMERICAL RESULTS AND DISCUSSION

In this section, a few FEM results are compared with the exact solution provided by Heyliger and Saravanos [23].

A three-layer thin square plate of unitary side ($a=1$(m)) loaded by a sinusoidal unitary pressure at the top face ($\widehat{p}_z=1(\mathrm{N/m^2})$) is considered in the following mechanical assessment. The plate is simply supported at the two opposite sides with zero pressure (cylindrical bending). The layers are of equal thickness and they are made of the same orthotropic material. The total thickness ratio is $a/h=100$ and the lamination scheme is [0/90/0]. Material

DOI: 10.1002/nme

Table III. Comparison between FEM and 3D-exact solutions, sensor case. LD2 and LM2 FEs are employed for PVD and RMVT case, respectively.

	$D_z \times 10^{13}$			
Height	3D [24]	RMVT-D_z	PVD	RMVT-D_z^*
1.000	160.58	160.22	239.57	234.38
0.975	149.35	148.27	204.92	203.62
0.950	117.23	117.53	161.38	163.98
0.925	66.568	68.003	108.95	115.44
0.900	−0.3382	−0.3044	47.621	58.008
0.900	−0.3382	−0.3044	−0.2990	−0.3101
0.800	−0.1276	−0.0969	−0.0977	−0.1027
0.700	0.0813	0.1064	0.1037	0.1048
0.600	0.2913	0.3058	0.3051	0.3123
0.500	0.5052	0.5010	0.5065	0.5198
0.500	0.5052	0.5010	0.4943	0.4815
0.400	0.7259	0.7228	0.7236	0.7165
0.300	0.9563	0.9495	0.9529	0.9515
0.200	1.1995	1.1812	1.1821	1.1865
0.100	1.4587	1.4179	1.4114	1.4215
0.100	1.4587	1.4179	−50.162	−58.915
0.075	−58.352	−59.178	−105.53	−111.00
0.050	−103.66	−103.15	−152.63	−154.82
0.025	−132.40	−130.50	−191.45	−190.36
0.000	−142.46	−141.23	−222.00	−217.63

The electric displacement is in (c/m^2). $D_z = D_z(a/2, b/2)$. The D_z RMVT-D_z^* is calculated by constitutive relations in the RMVT-D_z analysis.

properties are: $E_1 = 25,\ E_2 = 1,\ E_3 = 1,\ G_1 = 0.5,\ G_2 = 0.5,\ G_3 = 0.2$ (all in (GPa)); $v_{12} = 0.25$, $v_{13} = 0.25,\ v_{25} = 0.25$. Since the plate is very thin, the reduced integration technique has been preserved in order to overcome the shear locking phenomena. Convergence results concerning the midplane transverse displacement at the center of the plate are shown in Figure 1 for LMn and EDn Q4 FEs (Q4 states for four-nodes Quadrangular FEs). Regular $n \times 1$ meshes are considered. The following remark can be made. LMn FEs have good convergency properties. It can be noticed that, even when calculating a displacement, simple FEs like ED1 and ED2 converge to a value different from the 3D solution. Such difference decreases as the order of the thickness expansion increases. The obtained convergence properties are preserved for electrical quantities, when piezoelectric materials are included in the lamination. For the sake of conciseness this analysis is not quoted.

A simply supported cross-ply [0/90] laminate composed of an elastic material with piezoelectric layers bonded to the upper and lower surfaces is considered for the following electromechanical case study. The elastic layer of the [0] fiber angle is on the top. The plate is square with a side length a. The total thickness is h. The elastic layers have a thickness of $0.4h$, while the thickness of the piezoelectric layers is $0.1h$. The plate aspect ratio is $a/h = 4$. The elastic material is modeled as a fiber-reinforced composite and has the properties $E_{11} = 132.38$ (all in (GPa)), $E_{22} = 10.756,\ E_{33} = 10.756,\ G_{44} = 3.606,\ G_{55} = 5.654,\ G_{66} = 5.654,\ v_{12} = 0.24,$

DOI: 10.1002/nme

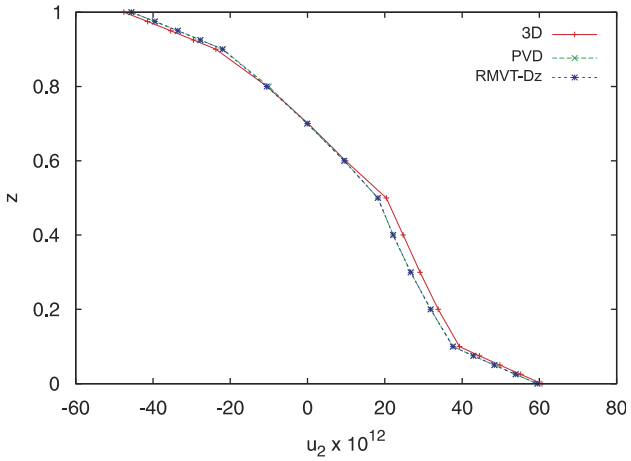

Figure 3. Comparison between LD2 FEM and 3D-exact solutions, sensor case; displacements are in (m); $u_2 = u_2(a/2, 0)$.

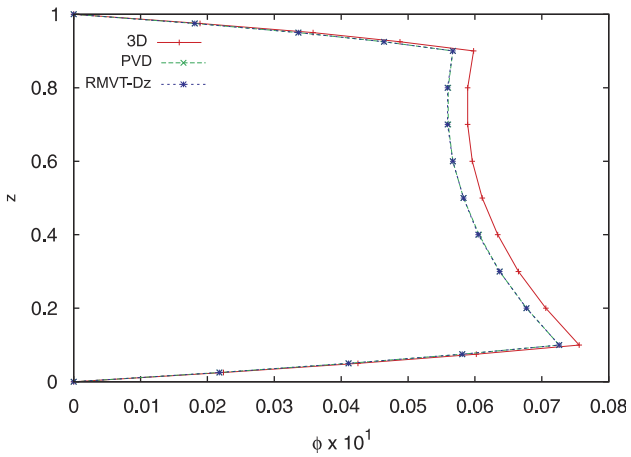

Figure 4. Comparison between LD2 FEM and 3D-exact solutions, sensor case; electric potential is in (V); $\phi = \phi(a/2, b/2)$.

$\nu_{13} = 0.24$, $\nu_{23} = 0.49$, $\varepsilon_{11}/\varepsilon_0 = 3.5$ and $\varepsilon_{22}/\varepsilon_0 = \varepsilon_{33}/\varepsilon_0 = 3.0$. The material of the piezoelectric layers is PZT-4 and the material properties are $E_{11} = E_{22} = 81.3$ (all in (GPa)), $E_{33} = 64.5$, $G_{44} = G_{55} = 25.6$, $G_{66} = 30.6$, $\nu_{12} = 0.329$, $\nu_{13} = \nu_{23} = 0.432$, $e_{31} = e_{32} = -5.20$ (all in (C/m^2)), $e_{33} = 15.08$, $e_{24} = e_{15} = 12.72$, and $\varepsilon_{11}/\varepsilon_0 = \varepsilon_{11}/\varepsilon_0 = 1475$, $\varepsilon_{33}/\varepsilon_0 = 1300$. The piezoelectric layer thickness is taken as 0.1 (m). Both the sensor case and actuator case are considered in the following (see the two configuration in Figure 2, where p_z indicates a pressure (N/m^2) and ϕ_t indicates the potential $[V]$ imposed on the top face and $\widehat{p_z} = \widehat{\phi}_t = 1$). The analysis will be restricted to LW cases. These last are, in fact, capable of furnishing reliable results at each layer interface. A second-order thickness expansion is considered to properly calculate the through-the-thickness

DOI: 10.1002/nme

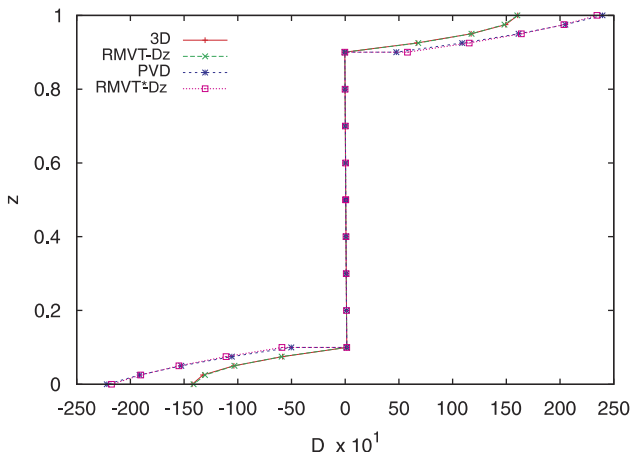

Figure 5. Comparison between FEM and 3D-exact solutions, sensor case; the electric displacement is in (c/m^2); $D_3 = D_3(a/2, b/2)$; the D_z RMVT-D_z^* is calculated by constitutive relations in the RMVT-D_z analysis.

electric displacement, which clearly shows a parabolic-like trend through the external layers (see Figure 5).

6.1. Sensor case

The applied double sinusoidal pressure loading p_z is considered on the top plate surface (sensor configuration). The load amplitude is equal to 1 (N/m^2). The top and bottom laminate surfaces are fixed at zero potential. The FEM results are obtained with a regular 10×10 mesh of LD2 (or LM2) Q4 FEs to minimize computational costs keeping a good accuracy. The exact midplane transverse displacement at the center of the plate is 30.027 (m), while the value calculated by the LD2 or LM2 FEs is 30.119 (m). Additional comparisons between the exact solution [24] and the FEM results are shown in Tables I–III and in Figures 3–5.

A comparison between the 3D-exact solution, PVD and RMVT-D_z results is provided in Table I for displacement u_2 and for the electric potential ϕ: the PVD and RMVT-D_z results are very close and they are in good agreement with the exact solution (see also Figures 3 and 4). In other words, when D_z is modeled by RMVT, the calculated primary variables do not change significantly with respect to PVD. However, if a slight difference is detected, the RMVT results are closer to the exact solution.

A comparison between the 3D-exact solution, PVD and RMVT-D_z results is provided in Table II for the transverse stress σ_{33} and for the in-plane stresses σ_{22} and σ_{12}: the PVD and RMVT-D_z results are close to the exact solutions. It has been confirmed that, even for stresses, the difference between PVD and RMVT-D_z is negligible.

The advantages of RMVT-D_z implementation are evident in Table III, where the evaluation of transverse displacement is referred to. The results are compared with 3D-exact and to PVD solutions. It should be underlined that RMVT-D_z leads to an almost 3D-exact description, while PVD results can be affected by very large errors (see also Figure 5). In the RMVT-D_z^* column, the D_z is calculated by using the physical constitutive relations in the RMVT-D_z analysis. It can be noted that the RMVT-D_z^* results are very close to the PVD ones.

DOI: 10.1002/nme

Table IV. Comparison between PVD and RMVT-D_z results, sensor case. LD2 or LM2 FEs are employed. Q is the charge at the top surface of the top layer and it is expressed in (c). RMVT-D_z^* result is computed starting from the D_z calculated by constitutive relations in the RMVT-D_z analysis.

$Q \times 10^{11}$(RMVT-D_z)	$Q \times 10^{11}$(PVD)	$Q \times 10^{11}$($RMVT$-D_z^*)
10.219	8.8763	8.5457

Table V. PVD and RMVT-D_z results: comparison between LD2 and LM2 FEM solutions with the 3D-exact solution, actuator case.

	$u_2 \times 10^{12}$	$u_2 \times 10^{12}$	$u_2 \times 10^{12}$	$\phi \times 10^{1}$	$\phi \times 10^{1}$	$\phi \times 10^{1}$
Height	3D [24]	PVD	RMVT-D_z	3D [24]	PVD	RMVT-D_z
1.000	−32.764	−33.951	−33.951	1.0000	1.0000	1.0000
0.975	−23.349	−24.377	−24.377	0.9971	0.9972	0.9972
0.950	−13.973	−14.826	−14.826	0.9950	0.9951	0.9951
0.925	−4.6174	−5.2983	−5.2977	0.9936	0.9936	0.9936
0.900	4.7356	4.2064	4.2069	0.9929	0.9929	0.9929
0.800	2.9808	2.5445	2.5448	0.8415	0.8423	0.8422
0.700	1.7346	1.2546	1.2548	0.7014	0.7011	0.7011
0.600	0.8008	0.3368	0.3368	0.5707	0.5695	0.5695
0.500	0.0295	−0.2091	−0.2091	0.4476	0.4473	0.4475
0.400	−0.4404	−0.5745	−0.5745	0.3305	0.3310	0.3311
0.300	−0.8815	−0.9518	−0.9517	0.2179	0.2177	0.2177
0.200	−1.3206	−1.3409	−1.3408	0.1081	0.1073	0.1073
0.100	−1.7839	−1.7419	−1.7418	−0.0001	−0.0001	−0.0001
0.075	−2.0470	−1.9963	−1.9963	−0.00009	−0.00009	−0.00009
0.050	−2.3140	−2.2554	−2.2554	−0.00008	−0.00007	−0.00007
0.025	−2.5856	−2.5191	−2.5191	−0.00004	−0.00004	−0.00004
0.000	−2.8625	−2.7875	−2.7876	0.00000	0.00000	0.00000

Displacements are in (m); electric potential is in (V). $u_2 = u_2(a/2, 0)$; $\phi = \phi(a/2, b/2)$.

The charge Q, calculated on the top surface of the top layer of the plate, under plate surface integration of D_z, according to Equation (1), is shown in Table IV. It is important to underline that RMVT-D_z provides a different charge value from PVD (almost 15% different) and this would encourage the use of RMVT-D_z, which appears mandatory in the sensor case.

6.2. Actuator case

The applied double sinusoidal potential p_z is considered in the top plate surface (actuator configuration). The load amplitude is equal to 1 (V). The bottom laminate surfaces are fixed at zero potential. The FEM results are obtained with a regular 10×10 mesh of LD2 (or LM2) Q4 FEs. The exact midplane transverse displacement at the center of the plate is -14.711×10^{-12} (m), while the value calculated by the LD2 and LM2 FEs is -14.151×10^{-12} (m) and -14.152×10^{-12} (m), respectively. Other comparisons between the exact solution [24] and the FEM results are shown in Tables V–VII.

DOI: 10.1002/nme

Table VI. PVD and RMVT-D_z results: comparison between LD2 and LM2 FEM solutions with the 3D-exact solution, actuator case.

	$\sigma_{33} \times 10^1$	$\sigma_{33} \times 10^1$	$\sigma_{33} \times 10^1$	σ_{22}	σ_{22}	σ_{22}	σ_{12}	σ_{12}	σ_{12}
Height	3D [24]	PVD	RMVT-D_z	3D [24]	PVD	RMVT-D_z	3D [24]	PVD	RMVT-D_z
1.000	0.0000	−55.800	−55.419	111.81	113.28	113.26	−146.03	−148.30	−148.30
0.975	−0.8333	−43.279	−43.183	63.736	66.186	66.175	−100.77	−103.03	−103.03
0.950	−2.8471	−28.385	−28.574	15.833	19.448	19.447	−55.693	−57.858	−57.855
0.925	−5.3241	−11.118	−11.592	−32.001	−26.932	−26.923	−10.698	−12.781	−12.778
0.900	−7.5482	8.5218	−7.7627	−79.865	−72.955	−72.935	34.295	32.198	32.221
0.900	−7.5482	−15.579	−15.581	−51.681	−68.096	−68.104	6.3365	5.9489	5.9494
0.800	−12.957	−11.567	−11.569	−33.135	−41.748	−41.753	4.6631	4.2950	4.2954
0.700	−15.245	−11.713	−11.714	−19.840	−21.342	−21.345	3.3247	2.9062	2.9064
0.600	−15.510	−16.014	−16.016	−9.7737	−6.8792	−6.8808	2.2096	1.7823	1.7825
0.500	−14.612	−24.473	−24.475	−1.3905	1.6408	1.6397	1.2286	0.9237	0.9238
0.500	−14.612	−17.335	−17.337	−1.3089	−1.2973	−1.2975	1.2287	0.9237	0.9238
0.400	−12.524	−12.937	−12.939	−0.5782	−3.3075	−3.3091	0.5227	0.3400	0.3401
0.300	−9.2558	−9.2086	−9.2096	0.1348	5.7883	5.7872	−0.0572	−0.1927	−0.1926
0.200	−5.5018	−6.1487	−6.1495	0.8463	1.4314	1.4313	−0.5840	−0.6744	−0.6744
0.100	−1.8733	−3.7579	−3.7583	1.5723	2.2270	2.2270	−1.1220	−1.1051	−1.1051
0.100	−0.8733	−3.3555	−2.8333	14.529	14.007	13.988	−6.0731	−5.9813	−5.9814
0.075	−1.1074	−4.1098	−3.7838	17.801	17.041	17.030	−7.3455	−7.1917	−7.1918
0.050	−0.5162	−4.3795	−4.2493	21.098	20.148	20.144	−8.6346	−8.4220	−8.4222
0.025	−0.1351	−4.1645	−4.2299	24.428	23.328	23.331	−9.9437	−9.6723	−9.6726
0.000	0.0000	−3.4647	−3.7256	27.795	26.581	26.591	−11.276	−10.942	−10.943

Stresses are in (Pa). $\sigma_{33} = \sigma_{33}(a/2, b/2)$; $\sigma_{11} = \sigma_{11}(a/2, b/2)$; $\sigma_{12} = \sigma_{12}(0, 0)$.

DOI: 10.1002/nme

Table VII. Comparison upon FEM solutions, actuator case. LD2 and LM2 FEs are employed for PVD and RMVT case, respectively.

	$D_z \times 10^{13}$		
Height	RMVT-D_z	PVD	RMVT-D_z^*
1.000	−2.4431	−2.4382	−2.4385
0.975	−1.8416	−1.8388	−1.8388
0.950	−1.2408	−1.2395	−1.2394
0.925	−6.4070	−6.4043	−6.4007
0.900	−4.1321	−4.1504	−4.0924
0.900	−4.1321	−4.1274	−4.1294
0.800	−3.8746	−3.8751	−3.8757
0.700	−3.6205	−3.6228	−3.6220
0.600	−3.3700	−3.3705	−3.3682
0.500	−3.1229	−3.1182	−3.1145
0.500	−3.1229	−3.1275	−3.1313
0.400	−3.0498	−3.0492	−3.0515
0.300	−2.9732	−2.9709	−2.9718
0.200	−2.8931	−2.8925	−2.8920
0.100	−2.8095	−2.8142	−2.8123
0.100	−2.8095	−2.8425	−2.8823
0.075	−2.8409	−2.8144	−2.8393
0.050	−2.8384	−2.7898	−2.7997
0.025	−2.8020	−2.7685	−2.7635
0.000	−2.7316	−2.7507	−2.7307

The electric displacement is in (c/m^2). $D_z = D_z(a/2, b/2)$. The D_z RMVT-D_z^* is calculated by constitutive relations in the RMVT-D_z analysis.

The following remarks can be made. Table V shows that the primary variables, u_2 and ϕ, calculated by FEM are in good agreement with the exact solution provided by Heyliger [24]. As far as Table VI is concerned, the in-plane stresses are also calculated with good accuracy, while the normal stress does not have reasonable values around the top and the bottom face of the plate. It is clear from Table VII that the RMVT-D_z modeling, compared with the PVD modeling, does not significantly improve the solution for the actuator case.

7. CONCLUSIONS

A new mixed variational statement (RMVT-D_z) is proposed in this work for the '*a priori*' evaluation of the transverse electric displacement D_z. FE plate elements have been developed to asses the numerical performance of RMVT-D_z. The numerical results clearly show that RMVT-D_z is capable of furnishing almost 3D-results for the D_z. For the sensor case, worse evaluations of D_z are instead obtained by using other variational statements, which discard the interlaminar continuity of D_z. In short, the RMVT-D_z should be preferred to other variational statements when fast and accurate results are needed for the prediction of D_z and of the electrical charge Q on the plate. Future work could be devoted to consider additional lay-out, boundary conditions and load cases.

DOI: 10.1002/nme

APPENDIX A: EXPLICIT FORMS OF RMVT-D_z FUNDAMENTAL NUCLEI

The stiffness fundamental nucleus $\mathbf{K}^{k\tau sij}$ related to the RMVT-D_z application is listed below. Constitutive information is included too. In the following, the layer-superscript k is always implied to simplify equations.

The stiffness fundamental nucleus is:

$$\mathbf{K}^{\tau sij} = \begin{bmatrix} K_{11} & K_{12} & K_{13} & K_{14} & K_{15} \\ K_{21} & K_{22} & K_{23} & K_{24} & K_{25} \\ K_{31} & K_{32} & K_{33} & K_{34} & K_{35} \\ K_{41} & K_{42} & K_{43} & K_{44} & K_{45} \\ K_{51} & K_{52} & K_{53} & K_{54} & K_{55} \end{bmatrix} \tag{A1}$$

Its elements are:

$$\begin{aligned}
K_{11} &= \widetilde{\mathbf{H}}_{aa}(7,7) \lhd N_i N_j \rhd_{\Omega_k} F_{\tau,z} F_{s,z} + \widetilde{\mathbf{H}}_{aa}(1,1) \lhd N_{i,x} N_{j,x} \rhd_{\Omega_k} F_\tau F_s \\
&\quad + \widetilde{\mathbf{H}}_{aa}(3,1) \lhd N_{i,y} N_{j,x} \rhd_{\Omega_k} F_\tau F_s \\
&\quad + \widetilde{\mathbf{H}}_{aa}(1,3) \lhd N_{i,x} N_{j,y} \rhd_{\Omega_k} F_\tau F_s + \widetilde{\mathbf{H}}_{aa}(3,3) \lhd N_{i,y} N_{j,y} \rhd_{\Omega_k} F_\tau F_s \\
K_{21} &= \widetilde{\mathbf{H}}_{aa}(8,7) \lhd N_i N_j \rhd_{\Omega_k} F_{\tau,z} F_{s,z} + \widetilde{\mathbf{H}}_{aa}(3,1) \lhd N_{i,x} N_{j,x} \rhd_{\Omega_k} F_\tau F_s \\
&\quad + \widetilde{\mathbf{H}}_{aa}(2,1) \lhd N_{i,y} N_{j,x} \rhd_{\Omega_k} F_\tau F_s \\
&\quad + \widetilde{\mathbf{H}}_{aa}(3,3) \lhd N_{i,x} N_{j,y} \rhd_{\Omega_k} F_\tau F_s + \widetilde{\mathbf{H}}_{aa}(2,3) \lhd N_{i,y} N_{j,y} \rhd_{\Omega_k} F_\tau F_s \\
K_{31} &= \widetilde{\mathbf{H}}_{aa}(7,7) \lhd N_{i,x} N_j \rhd_{\Omega_k} F_\tau F_{s,z} + \widetilde{\mathbf{H}}_{aa}(8,7) \lhd N_{i,y} N_j \rhd_{\Omega_k} F_\tau F_{s,z} \\
&\quad + \widetilde{\mathbf{H}}_{aa}(6,1) \lhd N_i N_{j,x} \rhd_{\Omega_k} F_{\tau,z} F_s \\
&\quad + \widetilde{\mathbf{H}}_{aa}(6,3) \lhd N_i N_{j,y} \rhd_{\Omega_k} F_{\tau,z} F_s \\
K_{41} &= -\widetilde{\mathbf{H}}_{aa}(4,7) \lhd N_{i,x} N_j \rhd_{\Omega_k} F_\tau F_{s,z} - \widetilde{\mathbf{H}}_{aa}(5,7) \lhd N_{i,y} N_j \rhd_{\Omega_k} F_\tau F_{s,z} \\
K_{51} &= \widetilde{\mathbf{H}}_{ba}(1,1) \lhd N_i N_{j,x} \rhd_{\Omega_k} F_\tau F_s + \widetilde{\mathbf{H}}_{ba}(1,3) \lhd N_i N_{j,y} \rhd_{\Omega_k} F_\tau F_s \\
K_{12} &= \widetilde{\mathbf{H}}_{aa}(7,8) \lhd N_i N_j \rhd_{\Omega_k} F_{\tau,z} F_{s,z} + \widetilde{\mathbf{H}}_{aa}(1,3) \lhd N_{i,x} N_{j,x} \rhd_{\Omega_k} F_\tau F_s \\
&\quad + \widetilde{\mathbf{H}}_{aa}(3,3) \lhd N_{i,y} N_{j,x} \rhd_{\Omega_k} F_\tau F_s \\
&\quad + \widetilde{\mathbf{H}}_{aa}(1,2) \lhd N_{i,x} N_{j,y} \rhd_{\Omega_k} F_\tau F_s + \widetilde{\mathbf{H}}_{aa}(3,2) \lhd N_{i,y} N_{j,y} \rhd_{\Omega_k} F_\tau F_s \\
K_{22} &= \widetilde{\mathbf{H}}_{aa}(8,8) \lhd N_i N_j \rhd_{\Omega_k} F_{\tau,z} F_{s,z} + \widetilde{\mathbf{H}}_{aa}(3,3) \lhd N_{i,x} N_{j,x} \rhd_{\Omega_k} F_\tau F_s \\
&\quad + \widetilde{\mathbf{H}}_{aa}(2,3) \lhd N_{i,y} N_{j,x} \rhd_{\Omega_k} F_\tau F_s \\
&\quad + \widetilde{\mathbf{H}}_{aa}(3,2) \lhd N_{i,x} N_{j,y} \rhd_{\Omega_k} F_\tau F_s + \widetilde{\mathbf{H}}_{aa}(2,2) \lhd N_{i,y} N_{j,y} \rhd_{\Omega_k} F_\tau F_s
\end{aligned}$$

DOI: 10.1002/nme

$$
\begin{aligned}
K_{32} &= \widetilde{\mathbf{H}}_{aa}(7,8)\lhd N_{i,x}N_j\rhd_{\Omega_k} F_\tau F_{s,z} + \widetilde{\mathbf{H}}_{aa}(8,8)\lhd N_{i,y}N_j\rhd_{\Omega_k} F_\tau F_{s,z} \\
&\quad + \widetilde{\mathbf{H}}_{aa}(6,3)\lhd N_i N_{j,x}\rhd_{\Omega_k} F_{\tau,z} F_s \\
&\quad + \widetilde{\mathbf{H}}_{aa}(6,2)\lhd N_i N_{j,y}\rhd_{\Omega_k} F_{\tau,z} F_s \\
K_{42} &= -\widetilde{\mathbf{H}}_{aa}(4,8)\lhd N_{i,x}N_j\rhd_{\Omega_k} F_\tau F_{s,z} - \widetilde{\mathbf{H}}_{aa}(5,8)\lhd N_{i,y}N_j\rhd_{\Omega_k} F_\tau F_{s,z} \\
K_{52} &= \widetilde{\mathbf{H}}_{ba}(1,3)\lhd N_i N_{j,x}\rhd_{\Omega_k} F_\tau F_s + \widetilde{\mathbf{H}}_{ba}(1,2)\lhd N_i N_{j,y}\rhd_{\Omega_k} F_\tau F_s \\
K_{13} &= \widetilde{\mathbf{H}}_{aa}(1,6)\lhd N_{i,x}N_j\rhd_{\Omega_k} F_\tau F_{s,z} + \widetilde{\mathbf{H}}_{aa}(3,6)\lhd N_{i,y}N_j\rhd_{\Omega_k} F_\tau F_{s,z} \\
&\quad + \widetilde{\mathbf{H}}_{aa}(7,7)\lhd N_i N_{j,x}\rhd_{\Omega_k} F_{\tau,z} F_s \\
&\quad + \widetilde{\mathbf{H}}_{aa}(7,8)\lhd N_i N_{j,y}\rhd_{\Omega_k} F_{\tau,z} F_s \\
K_{23} &= \widetilde{\mathbf{H}}_{aa}(3,6)\lhd N_{i,x}N_j\rhd_{\Omega_k} F_\tau F_{s,z} + \widetilde{\mathbf{H}}_{aa}(2,6)\lhd N_{i,y}N_j\rhd_{\Omega_k} F_\tau F_{s,z} \\
&\quad + \widetilde{\mathbf{H}}_{aa}(8,7)\lhd N_i N_{j,x}\rhd_{\Omega_k} F_{\tau,z} F_s \\
&\quad + \widetilde{\mathbf{H}}_{aa}(8,8)\lhd N_i N_{j,y}\rhd_{\Omega_k} F_{\tau,z} F_s \\
K_{33} &= \widetilde{\mathbf{H}}_{aa}(6,6)\lhd N_i N_j\rhd_{\Omega_k} F_{\tau,z} F_{s,z} + \widetilde{\mathbf{H}}_{aa}(7,7)\lhd N_{i,x}N_{j,x}\rhd_{\Omega_k} F_\tau F_s \\
&\quad + \widetilde{\mathbf{H}}_{aa}(8,7)\lhd N_{i,y}N_{j,x}\rhd_{\Omega_k} F_\tau F_s \\
&\quad + \widetilde{\mathbf{H}}_{aa}(7,8)\lhd N_{i,x}N_{j,y}\rhd_{\Omega_k} F_\tau F_s + \widetilde{\mathbf{H}}_{aa}(8,8)\lhd N_{i,y}N_{j,y}\rhd_{\Omega_k} F_\tau F_s \\
K_{43} &= -\widetilde{\mathbf{H}}_{aa}(4,7)\lhd N_{i,x}N_{j,x}\rhd_{\Omega_k} F_\tau F_s - \widetilde{\mathbf{H}}_{aa}(5,7)\lhd N_{i,y}N_{j,x}\rhd_{\Omega_k} F_\tau F_s \\
&\quad - \widetilde{\mathbf{H}}_{aa}(4,8)\lhd N_{i,x}N_{j,y}\rhd_{\Omega_k} F_\tau F_s \\
&\quad - \widetilde{\mathbf{H}}_{aa}(5,8)\lhd N_{i,y}N_{j,y}\rhd_{\Omega_k} F_\tau F_s \\
K_{53} &= \widetilde{\mathbf{H}}_{ba}(1,6)\lhd N_i N_j\rhd_{\Omega_k} F_\tau F_{s,z} \\
K_{14} &= -\widetilde{\mathbf{H}}_{aa}(7,4)\lhd N_i N_{j,x}\rhd_{\Omega_k} F_{\tau,z} F_s - \widetilde{\mathbf{H}}_{aa}(7,5)\lhd N_i N_{j,y}\rhd_{\Omega_k} F_{\tau,z} F_s \\
K_{24} &= -\widetilde{\mathbf{H}}_{aa}(8,4)\lhd N_i N_{j,x}\rhd_{\Omega_k} F_{\tau,z} F_s - \widetilde{\mathbf{H}}_{aa}(8,5)\lhd N_i N_{j,y}\rhd_{\Omega_k} F_{\tau,z} F_s \\
K_{34} &= -\widetilde{\mathbf{H}}_{aa}(7,4)\lhd N_{i,x}N_{j,x}\rhd_{\Omega_k} F_\tau F_s - \widetilde{\mathbf{H}}_{aa}(8,4)\lhd N_{i,y}N_{j,x}\rhd_{\Omega_k} F_\tau F_s \\
&\quad - \widetilde{\mathbf{H}}_{aa}(7,5)\lhd N_{i,x}N_{j,y}\rhd_{\Omega_k} F_\tau F_s \\
&\quad - \widetilde{\mathbf{H}}_{aa}(8,5)\lhd N_{i,y}N_{j,y}\rhd_{\Omega_k} F_\tau F_s \\
K_{44} &= \widetilde{\mathbf{H}}_{aa}(4,4)\lhd N_{i,x}N_{j,x}\rhd_{\Omega_k} F_\tau F_s + \widetilde{\mathbf{H}}_{aa}(5,4)\lhd N_{i,y}N_{j,x}\rhd_{\Omega_k} F_\tau F_s \\
&\quad + \widetilde{\mathbf{H}}_{aa}(4,5)\lhd N_{i,x}N_{j,y}\rhd_{\Omega_k} F_\tau F_s \\
&\quad + \widetilde{\mathbf{H}}_{aa}(5,5)\lhd N_{i,y}N_{j,y}\rhd_{\Omega_k} F_\tau F_s
\end{aligned}
$$

DOI: 10.1002/nme

$$K_{54} = \lhd N_i N_j \rhd_{\Omega_k} F_\tau F_{s,z}$$

$$K_{15} = -\widetilde{\mathbf{H}}_{ab}(1,1) \lhd N_{i,x} N_j \rhd_{\Omega_k} F_\tau F_s - \widetilde{\mathbf{H}}_{ab}(3,1) \lhd N_{i,y} N_j \rhd_{\Omega_k} F_\tau F_s$$

$$K_{25} = -\widetilde{\mathbf{H}}_{ab}(3,1) \lhd N_{i,x} N_j \rhd_{\Omega_k} F_\tau F_s - \widetilde{\mathbf{H}}_{ab}(2,1) \lhd N_{i,y} N_j \rhd_{\Omega_k} F_\tau F_s$$

$$K_{35} = -\widetilde{\mathbf{H}}_{ab}(6,1) \lhd N_i N_j \rhd_{\Omega_k} F_{\tau,z} F_s$$

$$K_{45} = \lhd N_i N_j \rhd_{\Omega_k} F_{\tau,z} F_s$$

$$K_{55} = -\widetilde{\mathbf{H}}_{bb}(1,1) \lhd N_i N_j \rhd_{\Omega_k} F_\tau F_s$$

Subscripts after comma indicates derivatives and:

$$\lhd (\ldots..) \rhd_{\Omega_k} = \int_{\Omega_k} (\ldots..)\, \mathrm{d}\Omega$$

The explicit form of matrices $\widetilde{\mathbf{H}}_{aa}, \widetilde{\mathbf{H}}_{ba}, \widetilde{\mathbf{H}}_{ab}$ and $\widetilde{\mathbf{H}}_{bb}$ is:

$$\widetilde{\mathbf{H}}_{aa} = \begin{bmatrix}
C_{11}+e_{31}^2/\varepsilon_{33} & C_{12}+e_{31}e_{32}/\varepsilon_{33} & C_{16}+e_{31}e_{36}/\varepsilon_{33} & 0 & 0 & C_{13}+e_{31}e_{33}/\varepsilon_{33} & 0 & 0 \\
C_{12}+e_{31}e_{32}/\varepsilon_{33} & C_{22}+e_{32}^2/\varepsilon_{33} & C_{26}+e_{32}e_{36}/\varepsilon_{33} & 0 & 0 & C_{23}+e_{32}e_{33}/\varepsilon_{33} & 0 & 0 \\
C_{16}+e_{31}e_{36}/\varepsilon_{33} & C_{26}+e_{32}e_{36}/\varepsilon_{33} & C_{66}+e_{36}^2/\varepsilon_{33} & 0 & 0 & C_{36}+e_{33}e_{36}/\varepsilon_{33} & 0 & 0 \\
0 & 0 & 0 & -\varepsilon_{11} & -\varepsilon_{12} & 0 & -e_{15} & -e_{14} \\
0 & 0 & 0 & -\varepsilon_{12} & -\varepsilon_{22} & 0 & -e_{25} & -e_{24} \\
C_{13}+e_{31}e_{33}/\varepsilon_{33} & C_{23}+e_{32}e_{33}/\varepsilon_{33} & C_{36}+e_{33}e_{36}/\varepsilon_{33} & 0 & 0 & C_{33}+e_{33}^2/\varepsilon_{33} & 0 & 0 \\
0 & 0 & 0 & -e_{15} & -e_{25} & 0 & C_{55} & C_{45} \\
0 & 0 & 0 & -e_{14} & -e_{24} & 0 & C_{45} & C_{44}
\end{bmatrix}$$

$$\widetilde{\mathbf{H}}_{ab}^{\mathrm{T}} = [e_{31}/\varepsilon_{33} \;\; e_{32}/\varepsilon_{33} \;\; e_{36}/\varepsilon_{33} \;\; 0 \;\; 0 \;\; e_{33}/\varepsilon_{33} \;\; 0 \;\; 0]$$

$$\widetilde{\mathbf{H}}_{ba} = [-e_{31}/\varepsilon_{33} \;\; -e_{32}/\varepsilon_{33} \;\; -e_{36}/\varepsilon_{33} \;\; 0 \;\; 0 \;\; -e_{33}/\varepsilon_{33} \;\; 0 \;\; 0]$$

$$\widetilde{\mathbf{H}}_{bb} = [-1/\varepsilon_{33}]$$

REFERENCES

1. Saravanos DA, Heyliger PR. Mechanics and computational models for laminated piezoelectric beams, plates, and shell. *Applied Mechanics Review* 1999; **52**(10):305–320.
2. Ji W, Yang J. High-order theories of piezoelectric plates and applications. *Applied Mechanics Review* 2000; **53**(4):87–96.
3. Sheikh AH, Topdar P, Halder S. An appropriate FE model for through-thickness variation of displacement and potential in thin moderately thick smart laminates. *Composite Structures* 2001; **51**:401–409.
4. Auricchio F, Bisegna P, Lovadina C. Finite element approximation of piezoelectric plates. *International Journal for Numerical Methods in Engineering* 2001; **50**:1469–1499.
5. Thornbuegh RP, Chattopadhyay A. Simultaneous modeling of mechanical and electrical response of smart composite structures. *AIAA Journal* 2002; **40**(8):1603–1610.

DOI: 10.1002/nme

6. Shu X. Free-vibration of laminated piezoelectric composite plates based on an accurate theory. *Composite Structures* 2005; **67**:375–382.
7. Oh J, Cho M. A finite element based on cubic zig-zag plate theory for the prediction of thermo-electric-mechanical behaviors. *International Journal of Solids and Structures* 2004; **41**(5–6):1357–1375. DOI: 10.1016/j.ijsolstr.2003.10.019.
8. Kogl M, Bucalem ML. Analysis of smart laminates using piezoelectric MITC plate and shell elements. *Computers and Structures* 2005; **83**:1153–1163.
9. Kogl M, Bucalem ML. A family of piezoelectric MITC plate elements. *Computers and Structures* 2005; **83**:1277–1297.
10. Carrera E. c_z^0 requirements—models for the two dimensional analysis of multilayered structures. *Composite Structures* 1997; **37**:373–383.
11. Reissner E. On a certain mixed variational theory and a proposed application. *International Journal for Numerical Methods in Engineering* 1984; **20**:1366–1368.
12. Reissner E. On a mixed variational theorem and on shear deformable plate theory. *International Journal for Numerical Methods in Engineering* 1986; **23**:193–198.
13. Carrera E. c^o Reissner–Mindlin multilayered plate elements including zig-zag and interlaminar stresses continuity. *International Journal for Numerical Methods in Engineering* 1996; **39**:1797–1820.
14. DeMasi L, Carrera E. Classical and advanced multilayered plate elements based upon PVD and RMVT. Part 1. Derivation of finite element matrices. *International Journal for Numerical Methods in Engineering* 2002; **55**: 191–231.
15. Carrera E. Theories and finite elements for multilayered plates and shells: a unified compact formulation with numerical assessment and benchmarking. *Archives of Computational Methods in Engineering* 2003; **10**:215–297.
16. Garcia Lage R, Mota Soares CM, Mota Soares CA, Reddy JN. Modeling of piezoelaminated plates using layerwise mixed finite elements. *Computers and Structures* 2004; **82**:1849–1863.
17. D'Ottavio M, Kröplin B. An extension of Reissner mixed variational theorem to piezoelectric laminates. *Mechanics of Advanced Materials and Structures* 2006; **13**(2):139–150.
18. Carrera E, Boscolo M. Classical and mixed finite elements for static and dynamics analysis of piezoelectric plates. *International Journal for Numerical Methods in Engineering* 2007; **70**:253–291.
19. Carrera E, Fagiano C. Mixed piezoelectric plate elements with continuous transverse electric displacements. *Journal of Mechanics of Materials and Structures* 2007; **2**(3):421–438.
20. Carrera E, Brischetto S, Nali P. Variational statements and computational models for multifield problems and multilayered structures. *Special Issue of MAMS* 2008; **15**(3):182–198.
21. Nellya DSc, Rogacheva L. *The Theory of Piezoelectric Shells and Plates*. CRC Press: Boca Raton, 1998.
22. Carrera E. An assessment of mixed and classical theories for the thermal stress analysis of orthotropic multilayered plates. *Journal of Thermal Stress* 2000; **23**:797–831.
23. Heyliger P, Saravanos DA. Exact free-vibration analysis of laminated plates with embedded piezoelectric layers. *Journal of Acoustical Society of America* 1995; **98**(3):1547–1557.
24. Heyliger P. Static behavior of laminated elastic–piezoelectric plates. *AIAA Journal* 1994; **32**(12):2481–2484.